Glass Transmitted Solar Irradiances on Horizontal and Sun-Normal Planes Evaluated with a Smartphone Camera

Adrian J. Dawes[1, 2], Damien P. Igoe[1], Katherine J. Rummenie[1] and Alfio V. Parisi[1, 2*]

[1]University of Southern Queensland, Faculty of Health, Engineering and Sciences, Toowoomba, Australia

[2]Centre for Applied Climate Sciences, University of Southern Queensland, Toowoomba, Australia

*To whom correspondence should be addressed

Alfio.Parisi@usq.edu.au

Abstract

This paper characterised and evaluated the ability of a smartphone camera to measure ultraviolet radiation (UVR) through various types and thicknesses of glass. Image sensor responses from a smartphone with UVA transmitting filters were measurably stronger in the red colour channel than the blue, with the green colour channel responding weakly. Strong correlations of up to R^2= 0.96 have been determined from calibration of the red and blue channel image responses against measured UVA irradiances for data obtained from both the horizontal plane and the sun-normal plane. For the validation data of the red channel and the blue channel respectively, the mean absolute error was 13.7% and 17.4% for the horizontal plane and 3.8% to 5.6% for the sun-normal plane. This research has concluded that it is possible to determine UVA irradiances through glass, of different thicknesses, using a smartphone camera with high degree of accuracy.

Keywords: UVA; glass; skin cancer; solar; irradiance

1. Introduction

Ultraviolet radiation (UVR) is long known to have both beneficial and detrimental effects on human biology. Balanced exposure to UVR can assist in the production of vitamin D, which has many benefits, including supporting the immune system, cardiovascular health and lung function, maintaining the health of bones and teeth, and assisting in the regulation of insulin [1]. Webb and Englesen [2] suggest that an adequate level of vitamin D protects the body against cancer development in the colon, prostate, and breast tissue. Underexposure to UVR may contribute to a range of biological and psychological developmental health problems due to the reduced production of vitamin D [1]. Overexposure to UVR contributes to cellular deterioration characterised by the production of cancerous cells in the basal, squamous, and melanocyte layers of the skin, generation of cataracts and optical keratosis [3,4], and is the leading cause of photoaging, through the degeneration of DNA replication [5].

Traditionally, UVR is measured using three main types of devices, specifically radiometers, spectrometers, and spectroradiometers [6], each of which has specific measurement qualities and output formats [7,8]. These devices have varying degrees of portability but are often too expensive for many research and occupational health and safety research groups. A common method of presenting information obtained from the standard devices is in the form of the UV index (UVI), which is predicted from a model based on accumulated data obtained from spectroradiometers and spectrometers projected into the future based on the assumption of cloud-free skies [4,9].

There have been many developments in relatively low cost UVR measurements, all with varying accuracy and reliability depending on calibration robustness [10]. An example of a relatively low cost and portable device to measure UVR is the *Solarmeter* (Solar Light Co., PA USA), which was found to have 5% to 10% agreement with a biometer and spectroradiometer at the Australian Radiation Protection and Nuclear Science Agency [11]. Recently, the use of inexpensive circuit and microcontroller kits (e.g. Raspberry Pi) have been calibrated and used for UV based observations, an example is [12] UVB observations of sulphur dioxide plumes using a Raspberry Pi based *PiCam*, calibrated with strong agreement ($R^2 = 0.92$) against a scientific grade UV camera.

There is a common public misconception that an individual can be protected from UVR exposure behind glass [6]. This is a potentially dangerous misconception as while normal window glass attenuates ultraviolet B (UVB: 280 nm – 320 nm) radiation, these wavebands are not completely absorbed until the glass thickness is greater than approximately 1.5 mm. Standard glass with a cross section of less than 1.5 mm will allow some UVB to pass through, with the cut-off wavelength decreasing as the glass thickness decreases [13]. The ultraviolet A (UVA: 320 nm – 400 nm) waveband is not as greatly affected by glass thickness; however, with the transmission irradiances for wavelengths longer than 360 nm showing less than 5% attenuation for glass as thick as 6.3 mm [14]. Previous research has established that it is possible to receive erythema (sunburn) through standard window glass if the exposure period is sufficiently long enough [15]. Previous research by Jelle et al. [16] has established metrics in an attempt to standardise photoprotective properties of building materials such as glass, including the solar material protection factor (SMPF) and solar skin protection factor (SSPF).

Primarily, the purpose of regular window glass is to permit the transmission of visible light into a structure while protecting against adverse and uncomfortable environmental conditions [17]. Standard window glass is created by heating silica (SiO_2) sand to melting point before being set into a useful form. Often, soda ash is added to the sand to decrease the melting temperature, while a non-soluble stabilising agent such as limestone is added to solidify the resultant material [18]. Along with these ingredients, a number of other chemicals can be added to the composition mainly to alter the material's resilience to heat, to heighten and alter the reflective properties of the material, to alter the colour of the material, and to absorb or transmit radiant energy of selected wavelengths [17-19]. The addition of these components invariably has an influence on the protective properties of the glass, altering the distribution of radiation passing through the material. Additional factors affecting radiation transmission include the application of embedded lamination layers and surface films [17], and multiple absorbance and reflectance profiles observed in multilayered glass [18]. In urban environments and vehicles, the most common types of glass used is classified as standard or normal glass, tinted glass, tempered or safety glass, and laminated glass [16,17,19].

Previous research has employed equipment such as dosimeters, radiometers and spectroradiometers for the measurement of UVR through glass [13,17,20-23]. No previous research has investigated employing the sensitivity to UVR of a smartphone camera for the measurement of glass transmitted UVR. This paper characterises and evaluates the ability of a

smartphone camera to measure the transmitted UVR through various types and thicknesses of glass. This characterisation and evaluation are used to determine the effect that optically dense materials may have on the ability of a smartphone camera image sensor to measure and monitor UVA irradiances in environments where direct illuminance is obscured.

2. Methodology

2.1 Location and times

All laboratory and field data were collected at the University of Southern Queensland campus in Toowoomba (27° 36' S, 151° 56' E), Australia. The approximate duration of each field data collection cycle was 5-7 minutes and up to 8 data cycles for both the horizontal plane and sun-normal plane were undertaken on any given data collection day.

The days when measurements were undertaken were selected to minimise the effects of optical obstructions such as the presence of clouds and aerosols. In total, 29 observation cycles across six days between late April and late July of 2018 were taken for calibration. The solar zenith angles (SZA) of these cycles ranged from approximately 45° to a maximum of 75°. A total of 23 observation cycles over the course of five days between late August 2018 and early April 2019 were collected for validation purposes. The SZA range for the validation data was between 17° and 68°.

2.2 Equipment and measurement method

Initial spectral transmission characteristics, from 280 nm to 800 nm, of all thicknesses and types of glass panes, and the filters used in this research were first measured in a UV spectrophotometer (model UV-VIS 2700, Shimadzu, Japan). This provided a baseline measurement, characterising the global transmission profile changes with glass thickness, as well as allowing observations of the effects of tints and laminates.

For each field observation cycle, the smartphone and radiometer (model PMA 2100, Solar Light Company, PA, USA) were arrayed so that both devices were able to be covered by the same sample glass slide. To eliminate as much as possible extraneous light in the visible and infrared wavebands, UG11 (Edmund Optics, Barrington, USA) and KG05 (SHOTT, Mainz,

Germany) filters were secured above the outer smartphone camera lens. Additionally, two neutral density (ND) filters (Bentham Instruments, Berkshire, UK) were attached above the filter array for sun-normal images to decrease saturation while measuring direct solar irradiances. Figure 1 displays the in-situ layout of the measurement apparatus in the sun-normal configuration. To ensure that the sun-normal data were collected in a direct path from the Sun to the apparatus a simple sun-targeting system was developed using a long cylindrical tube orientated parallel to the image collection direction. This tube was used to target the solar disk prior to the commencement of each sun-normal data collection cycle.

<Figure 1>

2.3 Data collection and analysis

Each observation point consisted of an image taken with the smartphone along with a simultaneous reading with the sunphotometer from beneath one of the sample glass panes. Between each of these datum points, the sample glass slides were exchanged in order, first for the horizontal plane and then for the sun-normal plane. A completed observation cycle, the point from which the process was repeated over, consisted of eight horizontal plane observations, followed by eight sun-normal plane observations. The order in which the glass slides were placed on the apparatus was clear glass samples, from 1 to 6 mm thickness, at 1 mm intervals; followed by the 6 mm laminated glass sample; and ending with the tinted glass samples (4 mm followed by 6 mm sample). Images were taken using a Sony Xperia Z1 (Sony Corporation, Tokyo, Japan) smartphone camera. The images were saved in the default JPEG format, typical for many smartphone models. This camera produced images with a resolution of 5248×3936 pixels. They were cropped prior to processing to minimise the effects of accidental light leakage. The initial cropping reduced 500 pixels from the outer edges of the original image, with images taken on a horizontal plane cropped by a further 500 pixels from the outer edges (1000 pixels total) to further minimise light leakage effects. The size of the images processed were thus:

Horizontal Plane: 3248×1936 pixels
Sun-normal plane: 4248×2936 pixels

The images were analysed using custom image processing *Python* programs. These programs were developed for the purpose of analysing smartphone images to determine for each image

the average pixel intensity value and standard deviation for each of the red, green, and blue colour channels [24]. This analysis is similar to the "Measure" function in the program *ImageJ* (https://imagej.net/) while permitting batch file processing to analyse multiple files. The number of pixels analysed by the sun-normal processing program varies according to the size of the solar disk represented in the image by a localised cluster of 'hot' or highly exposed pixels of the solar disk.

Once the average pixel value and standard deviation for each colour channel were obtained the average pixel value (C) was transformed according to the function in equation 1 [25,26].

$$C' = \ln\left(CD\cos^4\left(SZA\right)\right) \tag{1}$$

where C' is the transformed pixel values, calculated from the measured pixel values (C), the solar zenith angle (SZA), and the Sun-Earth distance correction factor (D) [27].

The transformed average pixel value for the red and blue channels (equation 1) from images taken from the horizontal and sun-normal planes were compared against observed broadband UVA irradiances. The green channel for the Sony Xperia Z1 had been previously identified as being indistinguishable from noise [26,28]. A second order polynomial regression was modelled for the horizontal plane data, while a linear regression was derived for the sun-normal plane data. Standard deviations of the pixel intensity value were used as an indicator of the relative noise of the image [29], indicated by error bars. The standard deviation distribution for both the horizontal and sun-normal plane observations were also compared to ascertain the relative significance of image sensor noise.

The signal to noise ratios (SNR) were determined by using a simplified transformation function [30,31], which is represented in equation 2.

$$\mathrm{SNR} = \frac{\mu - \mu_{dark}}{\sigma} \tag{2}$$

where μ and σ indicate the mean and standard deviation of C respectively. Dark current (μ_{dark}) has been identified as being a very minor source of noise in smartphones [26,32] thus is not considered for further analysis. The SNR is further expressed in decibels (dB) by equating $20\log_{10} SNR$ [30].

During initial image collection, it was found that irradiance saturation would occur in the red colour channel even with the use of multiple neutral density filters. This full saturation occurs when the brightness intensity of incident light is greater than the capacity of the sensor to record within the discrete numerical limit (8-bits, or digital values between 0-255 for image sensors in JPEG format). Full saturation is recorded as a pixel intensity value of 255 with a zero standard deviation. Pixel data that were determined to be oversaturated were removed prior to the calculation of calibration and validation models for the red colour channel, thus a smaller subset of data was analysed for this colour channel. The number of observations for each type and thickness of glass is presented in Table 1.

Table 1: Observations used for calibration and validation of the red colour channel data collected from the sun-normal plane orientation. These are a subset of the 29 total observations for each thickness and type of glass.

Number of utilised observations, red channel sun-normal data			
Calibration		Validation	
Glass sample type	Number of observations	Glass sample type	Number of observations
2 mm clear glass	21	2 mm clear glass	14
3 mm clear glass	23	3 mm clear glass	19
4 mm clear glass	23	4 mm clear glass	21
5 mm clear glass	25	5 mm clear glass	17
6 mm clear glass	25	6 mm clear glass	19
6 mm laminated glass	25	6 mm laminated glass	23
4 mm tinted glass	27	4 mm tinted glass	21
6 mm tinted glass	28	6 mm clear glass	22

3. Results and Discussion

3.1 Transmission characteristics

The spectral transmission of the glass panes and filters exhibited variations between glass sample types and thicknesses (Figure 2) and transmission properties of the filter arrangements demonstrated distinct profiles (Figure 3). The glass samples exhibited similarities in transmittance by glass composition type, with Figure 2 showing that the peak levels of transmittance decreased as the sample glass thickness increased. It was also observed that the minimum wavelength transmitted through glass increased as the thickness of standard glass increased, which is consistent with similar observations made by Parisi et al. [13]. The clear and tinted glass samples have a peak in transmittance in the UV spectrum at about 370 nm, while the laminated sample has a cut-off wavelength of about 370 nm, thus this peak was not evident. The maximum visible spectrum transmittance observed for the clear and laminated samples ranged from 480 nm to 580 nm, and transmittance past this point decreased at a rate related to the thickness of the glass sample, also consistent with previous research observations [13,14]. The transmission profile of the tinted glass samples is largely non-linear through the visible waveband with three major peaks up to 700 nm, along with two other minor peaks.

<Figure 2>

<Figure 3>

The difference in transmission profiles between the clear and tinted glass samples are most likely due to the material properties of the additives used to make the tint [16,17,19,33,34]. The laminated glass minimised transmission of UVA radiation, yet otherwise followed a similar transmission pattern to the normal glass samples. This was expected as the polyvinyl butyral (PVB) lamination is specifically identified as only blocking transmission of optical radiation below the UV-visible boundary [34].

The filter transmission profiles (Figure 3) demonstrated that combining the UG11 broadband transmission filter with the KG05 infrared blocking filter effectively blocked visible radiation transmission between the wavelengths of 400 nm to approximately 680 nm. Of the remaining radiation entering the smartphone camera aperture, approximately 98.5% of that radiation was in the UVA spectrum with the remainder being near infrared leakage, which has been previously observed in these types of filters [35]. When taking images on the sun-normal plane,

the two neutral density filters, ND2A and ND2B, were included in the filter array to minimise saturation of the image sensor. It was determined that these neutral density filters had a matching linear transmission regression that increased as wavelength increased (equation 3).

$$T_{ND2} = 0.006\lambda + 0.0747 \quad (3)$$

This transmission profile indicated that the neutral density filters transmitted 0.2% of incident radiation at 280 nm, increasing to about 4% at 800 nm. Consequently, using these filters slightly increased the relative amount of infrared radiation reaching the image sensor. The proportion of transmitted UVR received by the smartphone image sensor was 73.4%. This was accounted for in the calibration of the image sensor to the radiometer.

3.2 Horizontal plane

Horizontal plane images were observed to not include the solar disc during the calibration phase, displaying the predicted distinct second order polynomial regression (Figure 4). Hence, the relative image sensor noise increased with lower irradiances on the smartphone image sensors. Correlations were slightly stronger for the blue colour channel compared to the red colour channel when observing through clear glass, with maximum R^2 values of 0.95 and 0.93 respectively.

The general formula relating the horizontal plane data and measured UVA irradiances was a second order function. Variability, indicated by error bars in Figures 4 and 5, increased with lower irradiances incident on the smartphone sensors. The standard deviations, used to determine the relative noise, maintained a strong numerical stability, ranging from between 0.18 to 5.32 for the horizontal plane blue colour channel, regardless of the average pixel value (which ranged from 0.02 to 19.35). This suggests that low-level ambient noise was present in the smartphone image sensor, increasing the potential for error at low irradiances.

Known sources of noise obtained from digital imagery include off-set fixed pattern noise, gain fixed pattern noise, shot noise, readout noise, column noise, demosaicing, and quantisation [36]. Most of these noise sources are device and environment dependent and were not investigated directly in this research, as the noise is considered very low relative to high signal measured from the horizontal plane and sun-normal images. It is due to the negligible level of noise in images compared with a high signal that sun-normal image errors were relatively small

(Figure 5). The green colour channel signal was, in general, more than two orders of magnitude smaller than those received for the red and blue channels. Due to this, the relative noise of this channel was significantly higher than those of the other two channels. This characteristic is consistent with prior studies in smartphone sensor response to UVB radiation with the same smartphone [26,28]. The horizontal plane green channel had an average SNR of 0.82, indicating that the noise was too high to determine an effective regression for calibration. In comparison, the red colour channel had an average SNR of 2.12 while the blue channel had a similar average SNR of 2.18. For this reason, the green channel data was not used in any further analysis.

<Figure 4>

<Figure 5>

Some of the validation observations were obtained during local mid-summer when the solar disc became visible in the horizontal-plane images. These can be identified in Figure 4, plots c and d, as outliers to the right of the 1-to-1 relationship line, with the outliers correlating to UVA irradiances of between approximately 20 and 40 W/m^2. This indicates that the non-solar disc horizontal plane calibration models will tend to over-predict UVA irradiance values when there is a visible solar disc in the image. Additionally, there was a persistent over-prediction at high UVA irradiance levels, equitable to low SZA, suggesting a decrease in accuracy at low SZA. The mean absolute error for the validation of UVA irradiances through clear glass samples was lower for the blue than the red colour channel (maximum 13.7% and 17.4% respectively).

3.3 Sun-normal plane

Calibration and validation plots for the sun-normal plane observations are displayed for the red and blue colour channels in Figure 5, the green colour channel was omitted for the reasons previously explained. Linear regressions were found to be most appropriate for the sun-normal data as there was no noticeable curvature. The error bars in the sun-normal plane plots, while displayed, are largely insignificant.

These images were taken with the smartphone camera orientated directly at the sun so the image sensor response being measured was significantly higher than that obtained for

horizontal plane observations, even with the use of neutral density filters. The data obtained for the sun-normal plane indicated that there is a linear relationship in the response to UVA irradiance. The second order polynomial regressions determined for the horizontal plane observations were notably different from the linear regressions determined from the sun-normal plane observations (Figure 5), and from data obtained through prior study in this field [37]. The prior horizontal plane observations were found to be consistent with the sun-normal plane data from this earlier study, which can be accounted for by the visible presence of the solar disc in the smartphone images, also noted during the horizontal plane validation. It can be surmised that the regression functions obtained for the horizontal plane observations predominantly relate to diffuse irradiance only, while the presence of the sun in the sun-normal, horizontal-plane validation, and earlier observations made by Rummenie [37] are dominated by global (direct and diffuse) irradiances.

The regression fits of the sun-normal plane data were generally stronger than those obtained for the horizontal plane, with the clear glass irradiances having a very strong correlation for the red and blue colour channels (R^2 = 0.96 - 0.94). This higher correlation could be partly accounted for by the decreased number of utilised data points for each channel. The data were well-validated for all glass samples, with a mean absolute error ranging from 3.8% to 5.6%, again with less error observed in the red colour channel. Additionally, it was observed that there was a lower propensity of over-prediction in comparison to the horizontal plane images, as indicated in the validation plots (Figure 5, plots c and d), regardless of SZA.

4. Conclusion

The use of a smartphone camera was evaluated and validated as an effective means of gathering relevant glass-filtered UV irradiance information for scientific use and public awareness. Observations were undertaken for glass of different types and thicknesses on a horizontal plane and on a plane normal to the sun. A clear correlation was observed to exist between the broadband UVA glass-filtered irradiances and smartphone image sensor responses. Calibration of data from the analysed smartphone images to the transmitted irradiance indicated that there was high reliability, with an R^2 range of 0.91 to 0.96 for the horizontal and the sun-normal planes through clear glass samples. The mean absolute error for the validation of UVA irradiances through clear glass samples on a horizontal plane was 13.7% to 17.4% and from 3.8% to 5.6% for the sun-normal plane. Direct irradiances had a significant influence in

lowering the relative noise, as indicated by the considerably lower error for sun-normal observations when compared with the diffuse irradiances dominating the horizontal plane observations.

The reliability of data obtained from measurement through laminated glass was lower than for the other sample types due to minimal transmission of UVR. Tinted glass measurements were found to increase in reliability at lower SZA when measuring diffuse irradiance on the horizontal plane but showed stronger correlation for direct irradiance measurements from the sun-normal plane. The decrease in reliability appears to correlate with decreased image sensor responses due to low material UVR transmission.

This research has shown that it is possible to develop a relationship between a smartphone image sensor response to the UVA irradiances filtered through different types and thicknesses of glass used in buildings where people live and work, providing a viable and accessible public safety tool.

Funding: This research did not receive any specific grant from funding agencies in the public, commercial, or not-for-profit sectors.

References

[1] Lucas, R., McMichael, T., Smith, W., & Armstrong, B. (2006), "Solar ultraviolet radiation: Global burden of disease from solar ultraviolet radiation," Geneva: World Health Organisation.

[2] Webb, A. R., & Englesen, O. (2006), "Calculated ultraviolet exposure levels for a healthy vitamin D status," *Photochemistry and Photobiology*, 82, 1697-1703.

[3] Agar, N. S., Halliday, G. M., Barnetson, R., Ananthaswamy, H.N., Wheeler, M., & Jones, A. M. (2004), "The basal layer in human squamous tumours harbours more UVA than UVB fingerprint mutations: A role for UVA in human skin carcinogenesis," *Proc. Nat. Acad. Sci.* vol. 101, pp.4954-4959.

[4] WHO, (1994), Environmental Health Criteria 160: ultraviolet radiation, Geneva

[5] Takeuchi, H., & Runger, T. M. (2013), "Longwave UV Light Induces the Aging-Associated Progerin," Journal for Investigative Dermatology, 133, 1857-1862.

[6] Parisi, A. V., Sabburg, J., & Kimlin, M. G. (2004), *Scattered and Filtered Solar UV Measurements*, Dordrecht: Kluwer Academic Publishers.

[7] Ansko, I., Eerme, K., Latt, S., Noorma, M., & Veismann, U. (2008), "Study of suitability of AvaSpec array spectrometer for solar UV field measurements," *Atmospheric Physics and Chemistry*, 8, 3247-3253. doi:10.5194/acp-8-3247-2008

[8] Lakkala, K., Arola, A., Heikkila, A., Kaurola, J., Koskela, T., Kyro, E., & Hulsen, G. (2008), "Quality assurance of the Brewer spectral UV measurements in Finland," *Atmospheric Physics and Chemistry*, 8, 3369-3383. doi:10.5194/acp-8-3369-2008

[9] Meves, A., Repacholi, M. H., & Rehfuess, E. A. (2003), "Global Solar UV Index: a physician's tool for fighting the skin cancer epidemic," *International Journal of Dermatology*, 42, 486-489.

[10] Kanellis, V.G. (2019), "Ultraviolet radiation sensors: a review", *Biophysical Reviews*, 11, 895-899.

[11] Dobbinson, S., Niven, P., Buller, D., Allen, M., Gies, P., & Warne, C. (2015), "Comparing handheld meters and electronic dosimeters for measuring ultraviolet levels under shade and in the sun," *Photochemistry and Photobiology*, 92(1), 208-214.

[12] Wilkes, T.C., Pering, T.D., McGonigle, A. J. S., Tamburello, G., & Willmott, J. R. (2017), "A low-cost smartphone sensor-based UV camera for volcanic SO_2 emission measurements," *Remote Sensing*, 9, 27.

[13] Parisi, A. V., Turnbull, D. J., & Kimlin, M. G. (2007), "Dosimetric and spectroradiometric investigations of glass-filtered solar UV," *Photochemistry and Photobiology*, 83, 777-781. doi:10.1562/2006-08-20-RA-1007

[14] Tuchinda, C., Srivannaboon, S., & Lim, H. W. (2006, May), "Photoprotection by window glass, automobile glass, and sunglasses," *Journal of the American Academy of Dermatology*, 845-854.

[15] Schmalweiser, A. W. and Siani, A. M. (2018), "Review of non-occupational personal solar UV exposure measurements", *Photochemistry and Photobiology*, 94, 900-915.

[16] Jelle, B. P. (2013), "Solar radiation glazing factors for window panes, glass structures and electrochromic windows in buildings - Measurement and calculation," *Solar Energy Materials & Solar Cells*, 116, 291-323. doi:10.1016/j.solmat.2013.04.032

[17] Duarte, I., Rotter, A., Malvestiti, A., & Silva, M. (2009), "The role of glass as a barrier against the transmission of ultraviolet radiation: an experimental study," *Photodermatology, Photoimmunology & Photomedicine*, 25, 181-184.

[18] Jelle, B. P., Gustavsen, A., Nilsen, T. M., & Jacobsen, T. (2007), "Solar material protection factor (SMPF) and solar skin protection factor (SSPF) for window panes and other glass structures in buildings," *Solar Energy Materials and Solar Cells*, 91, 342-354.

[19] Jansen, R., Wang, S. Q., Burnett, M., Osterwalter, U., & Lim, H. W. (2013), "Photoprotection: Part I. Photoprotection by naturally occurring physical and systemic agents", *Journal of the American Academy of Dermatology*, 69, 853e1-853e12

[20] Gies, H. P., Roy, C. R., & Zongli, W. (1992), "Ultraviolet Radiation Protection Factors for Clear and Tinted Automobile Windscreens," *Radiation Protection in Australia*, 10(4), 91-94.

[21] Kimlin, M.G., Parisi, A.V., Carter, B.D., & Turnbull, D. (2002), "Comparison of the solar spectral ultraviolet irradiance in motor vehicles with windows in an open and closed position," *Int. J. Biometeorol.* vol.46, pp.150-156.

[22] Moehrle, M., Soballa, M., & Korn, M. (2003), "UV exposure in cars," *Photodermatology Photoimmunology & Photomedicine*, 19, 175-181.

[23] Parisi, A. V., & Kimlin, M. G. (2000), "Estimate of annual ultraviolet-A exposures in cars in australia," *Radiation Protection Dosimitry*, 90(4), 409-416, doi:10.1093/oxfordjournals.rpd.a033167

[24] Igoe, D., Parisi, A., & Carter, B. (2014), "Smartphone-Based Android app for Determining UVA Aerosol Optical Depth and Direct Solar Irradiances," *Photochemistry and Photobiology*, (90), 233-237. doi:10.1111/php.12185

[25] Igoe, D., Parisi, A. V., & Carter, B. (2014), "A method for determining the dark response for scientific imaging with smartphones," *Instrumentation Science and Technology*, 42, 586-592.

[26] Igoe, D. P., Amar, A., Parisi, A. V., & Turner, J. (2017), "Characterisation of a smartphone image sensor response to direct solar 305 nm irradiation at high air masses," *Science of the Total Environment*, 587-588, 407-413. doi:10.1016/j.scitotenv.2017.02.175

[27] Porter, J. N., Miller, M., Pietras, C., & Motell, C. (2001), "Ship-based sun photometer measurements using microtops sun photometers," *Journal of Atmospheric and Oceanic Technology*, 18, 765-774.

[28] Igoe, D., Parisi, A. V., Downs, N. P., Amar, A., & Turner, J. (2018), "Comparative signal to noise ratio as a determinant to select smartphone image sensor colour channels for analysis in the UVB," *Sensors and Actuators A: Physical*, 272, 125-133, doi: 10.1016/j.sna.2018.01.057

[29] Riutort-Mayol, G., Marqués-Mateu, A., Seguí, A. E. & Lerma, J. L. (2012), "Grey level and noise evaluation of a Foveon X3 image sensor: A statistical and experimental approach", *Sensors*, 12, 10339-10368. doi: 10.3390/s120810339

[30] European Machine Vision Association (EMVA), (2010), "Standard for Characterization of Image Sensors and Cameras", *EMVA*, Standard 1288, release 3.0

[31] Sijbers, J., Scheunders, P., Bonnet, N., Van Dyck, D., & Raman, E. (1996), "Quantification and improvement of the signal-to-noise ratio in a magnetic resonance image acquisition procedure," *Magnetic Resonance Imaging*, 14(10), 1157-1163.

[32] Burggraff, O., Schmidt, N., Zamorano, J., Pauly, K., Pascual, S., Tapia, C., Spyrakos, E. and Snik, F. (2019), "Standardized spectral and radiometric calibration of consumer cameras", *Optics Express*, 27, 19075-19101. doi: 10.1364/OE.27.019075

[33] Almutawa, F., & Buabbas, H. (2014), "Photoprotection Clothing and Glass", *Dermatol Clin*, 32. pp.439-448.

[34] Almutawa, F., Vandal, R., Wang, S. Q., & Lim, H. W. (2013), "Current status of photoprotection by window glass, automobile glass, window films, and sunglasses," *Photodermatology, Photoimmunology & Photomedicine*, 29, 65-72. doi:10.1111/phpp.12022

[35] Williams, R., & Williams, G. (2002), "Ultraviolet, infrared and fluorescence photography," Retreived August 24 2019, from Medical and Scientific Photography: http://www.medicalphotography.com.au/Article_01/06.html

[36] Irie, K., McKinnon, A. E., Unsworth, K., & Woodhead, I. M. (2008), "Measurement of digital camera image noise for imaging applications," *Sensors and Transducers*, 185-194.

[37] Rummenie, K. J. (2017), *Measurement of UVA through glass using a smartphone camera*, Unpublished report, Toowoomba, Queensland, Australia: University of Southern Queensland.

Figure Captions

Figure 1: *In situ* image of the data gathering equipment for a sample sun-normal measurement. Both the smartphone camera (B) and the UVA sensor (A) are arranged beneath the 2 mm clear glass sample slide. The sun targeting apparatus protrudes from the front of the array (C).

Figure 2: Transmission profile for sample glass panes from 280 nm to 800 nm.

Figure 3: The transmission profiles from 280 nm to 800 nm for the filters employed in this research.

Figure 4: Horizontal plane calibration and validation plots for red colour channel (left, a and c) and blue colour channel (right, b and d) data. Error bars indicate one standard deviation from the average pixel intensity values.

Figure 5: Sun-normal plane regression and validation for the mean red colour channel (left, a and c) and mean blue colour channel (right, b and d) data. Error bars indicate one standard deviation and are generally too small to be seen.

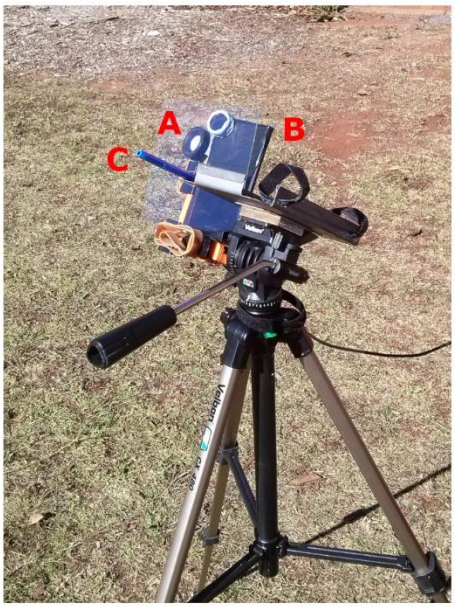

Figure 1: *In situ* image of the data gathering equipment for a sample sun-normal measurement. Both the smartphone camera (B) and the UVA sensor (A) are arranged beneath the 2 mm clear glass sample slide. The sun targeting apparatus protrudes from the front of the array (C).

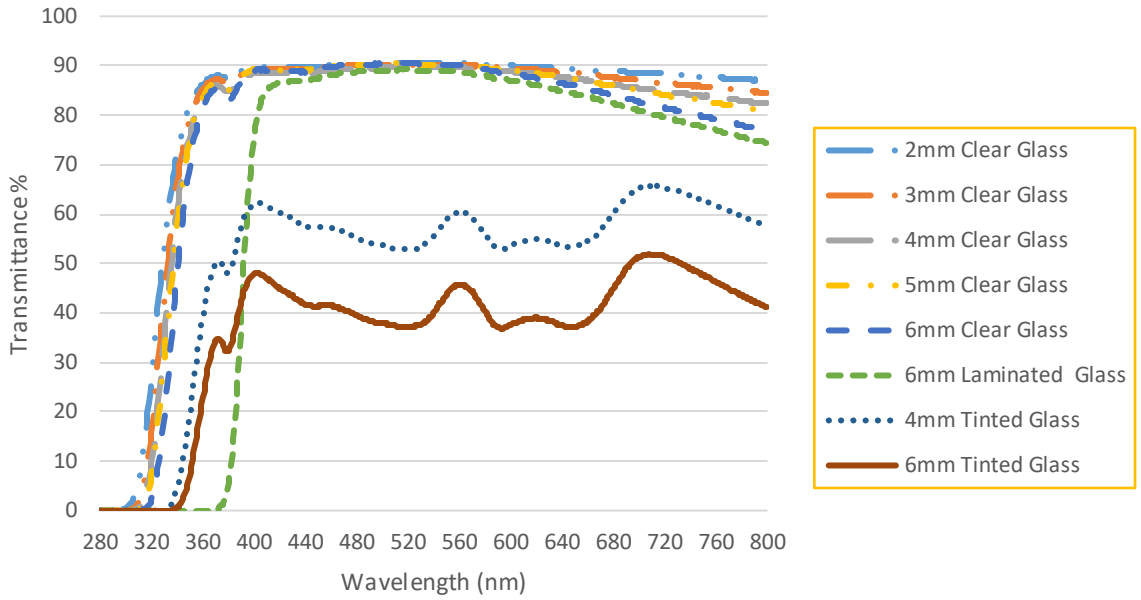

Figure 2: Transmission profile for sample glass panes from 280 nm to 800 nm.

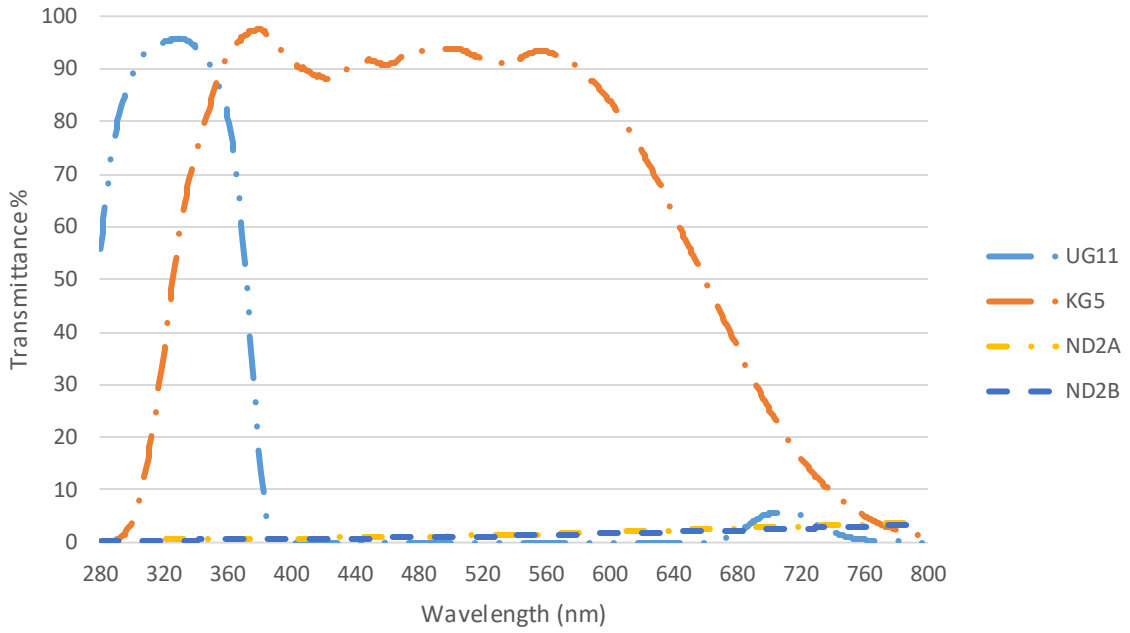

Figure 3: The transmission profiles from 280 nm to 800 nm for the filters employed in this research.

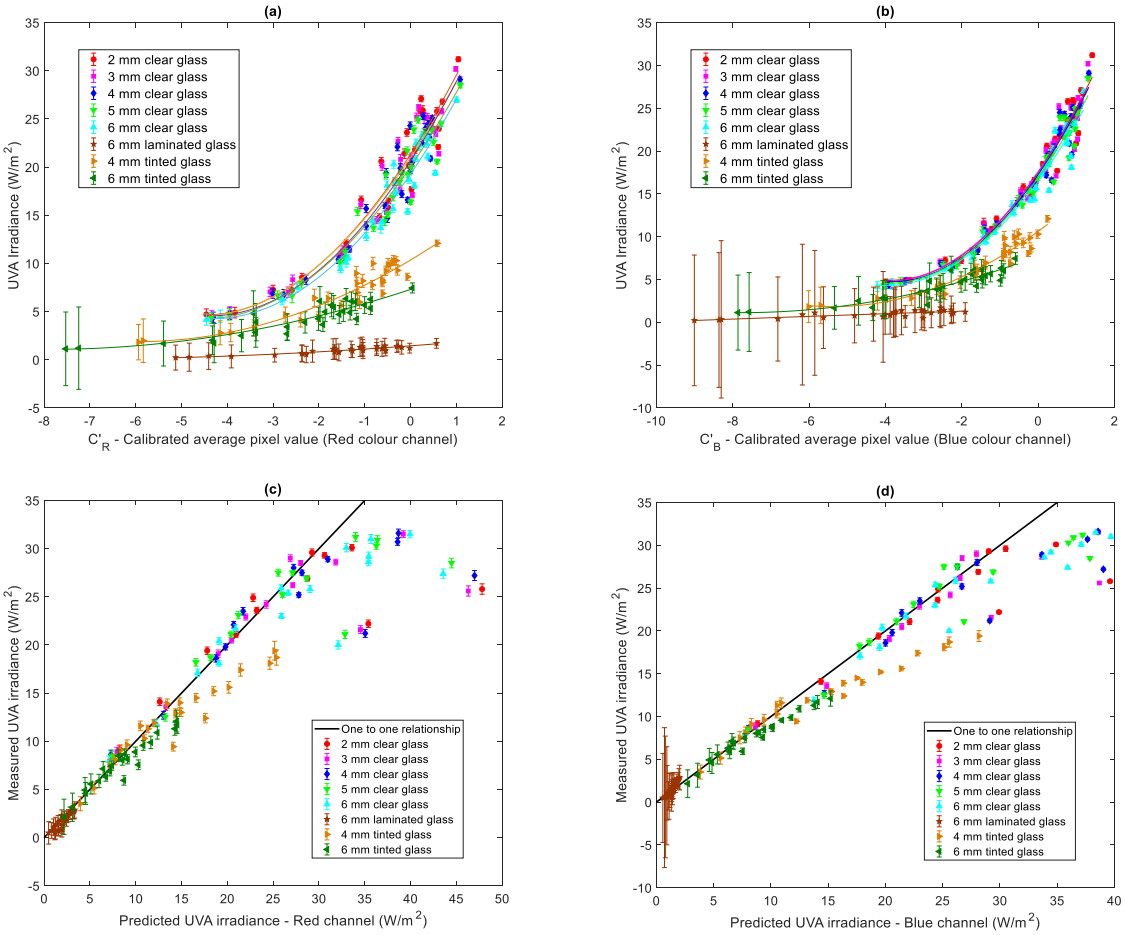

Figure 4: Horizontal plane calibration and validation plots for *r*ed colour channel (left, a and c) and blue colour channel (right, b and d) data. Error bars indicate one standard deviation from the average pixel intensity values.

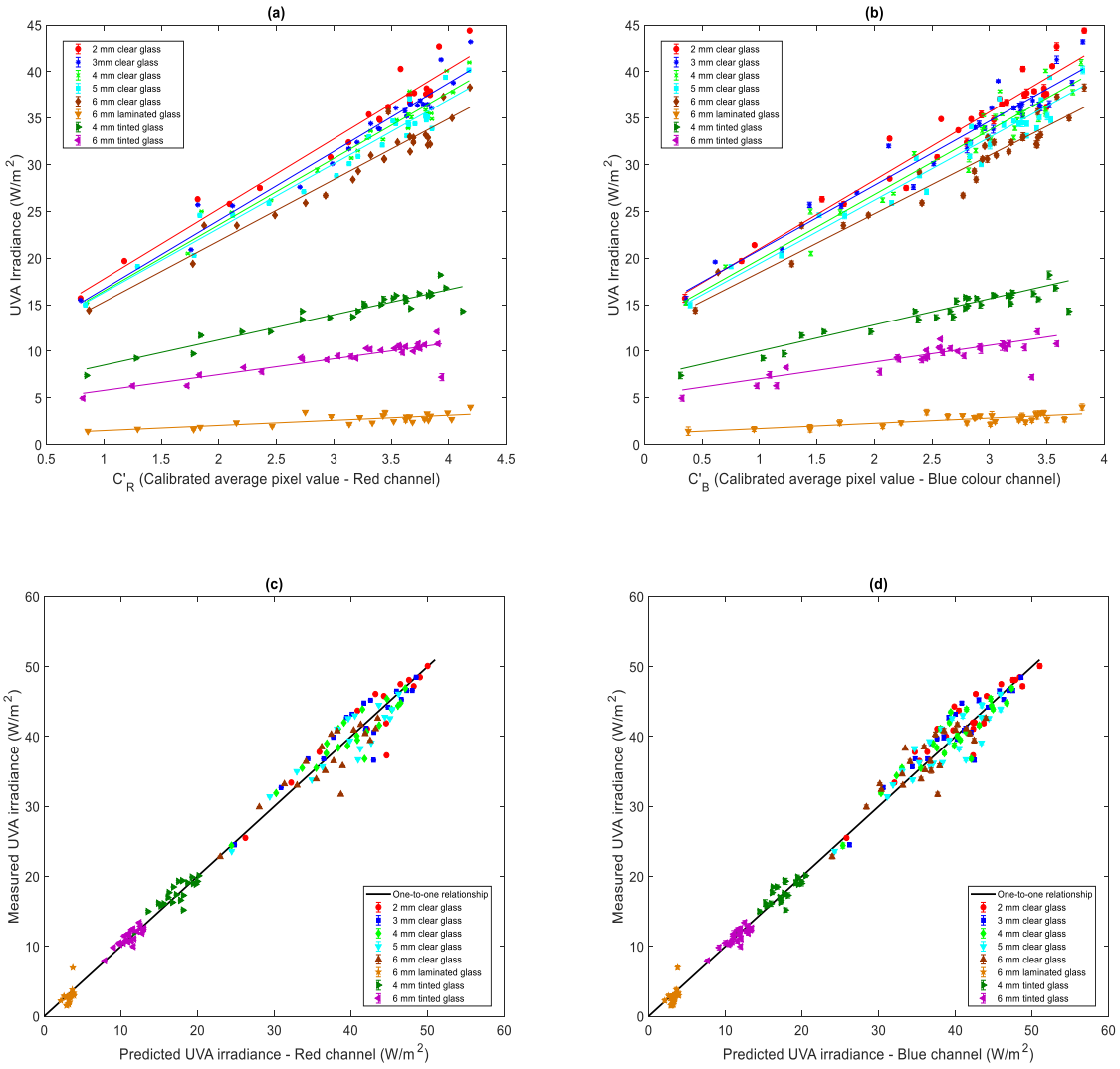

Figure 5: Sun-normal plane regression and validation for the mean red colour channel (left, a and c) and mean blue colour channel (right, b and d) data. Error bars indicate one standard deviation and are generally too small to be seen.